Characteristics of Thermo-Acoustic Emission from Composite Laminates during Thermal Load Cycles

Young-Bok Kim
Department of Mechanical Design, Hanyang University, Sungdong-koo, Seoul 133-791, Korea
Nak-Sam Choi*
Department of Mechanical Engineering, Hanyang University, 1271, Sa-1dong, Ansan-si, Kyunggi-do 425-791, Korea

The thermo-acoustic emission (AE) technique has been applied for nondestructive characterization of composite laminates subjected to cryogenic cooling. Thermo-AE events during heating and cooling cycles showed a Kaiser effect. An analysis of the thermo-AE behavior obtained during the 1st heating period suggested a method for determining the stress-free temperature of the composite laminates. Three different thermo-AE types classified by a short-time Fourier transform of AE signals enabled to offer a nondestructive estimation of the cryogenic damages of the composites, in that the different thermo-AE types corresponded to secondary microfracturing in the matrix contacting between crack surfaces and some abrasive contact between broken fiber ends during thermal load cycles.

Key Words: Thermo-Acoustic Emission, Composite Laminates, Kaiser Effect, Thermal Load Cycles, Short-Time Fourier Transform, Nondestructive Estimation

1. Introduction

Although fiber-reinforced composites have high modulus and high strength as well as superior vibration absorption ability in comparison to isotropic metals and alloys, damages such as microcracks, delaminations and/or warpage may occur due to the microstructural anisotropy formed during the manufacturing process and to the temperature variation under in-service conditions. These damages may lead to a considerable reduction in the strength and the expected service-life of composite components for aero-space structures, atomic reactors as well as electronic devices. Thus nondestructive detection and evaluation of the damages are important for the safety of fiber-composite structures.

Since acoustic emission (AE) technique detects stress waves which are generated by transient release of stored strain energy, material state and fracture mechanism have been evaluated in a nondestructive manner by analyzing AE data (Weng et. al., 1990; Choi et. al., 1992; Choi and Takahashi, 1998). The technique has also been applied to fiber-composites which are subjected to thermal load cycles (Sato et. al., 1988; Lee et. al., 1999; Choi and Lee, 2001). Although scarce in damage-free composites, numerous thermo-AEs were observed in the composites containing pre-existent damages caused by static and dynamic loads.

In this work, the thermo-AE technique is applied for nondestructive characterization of the fiber-composite laminates subjected to cryogenic cooling. The composite with layup of $[+45_6/-45_6]_s$ is adopted as a typical laminate for this study. Kaiser effect in thermo-AE behavior is investigated during thermal cycles. A method for determining a stress-free temperature is studied

* Corresponding Author,
E-mail: nschoi@hanyang.ac.kr
TEL: +82-31-400-5283; **FAX**: +82-31-406-5550
Department of Mechanical Engineering, Hanyang University, 1271, Sa-1dong, Ansan-si, Kyunggi-do 425-791, Korea. (Manuscript **Received** August 29, 2002; **Revised** December 14, 2002)

through thermo-AE analysis. Thermo-AE signals are quantitatively classified into different types through a short-time Fourier transform, utilized for the possibility of a nondestructive testing for cryogenic damage.

2. Experimental Procedure

2.1 Composite laminates and cryogenic cooling

Composite laminates of $[+45_6/-45_6]_s$ were made of a unidirectional carbon fiber/epoxy prepreg (Hankook Fiber Co.) with a thickness of 0.125 mm in an autoclave using the curing cycle as shown in Fig. 1. Temperature drop was performed from curing (170℃) to room temperature. Rectangular specimens (30 mm×100 mm ×3 mm) for cryogenic cooling were made by sectioning the laminate plate with a diamond wheel cutter as illustrated in Fig. 2. Each specimen was rapidly inserted into the cryogenic chamber filled with liquid nitrogen (−191℃) and kept there for 20 minutes.

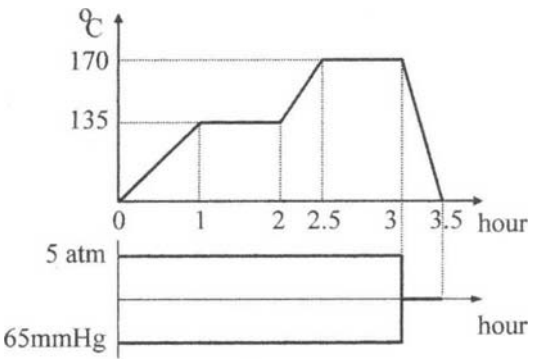

Fig. 1 Curing cycle of the composite plate

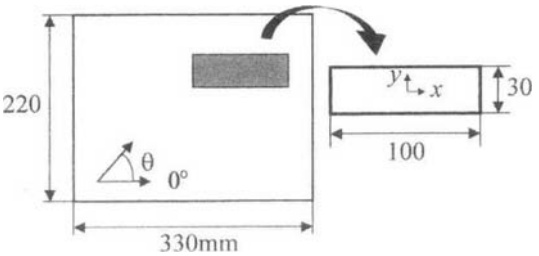

Fig. 2 Sectioning of a composite plate

2.2 Thermo-acoustic emission measurement

The specimen at room temperature was mounted on the one end of a wave guide beam by using vacuum silicone grease. An AE transducer (R15, Dunegan Corp.: detectable frequency range of 70~600 kHz, resonant frequency of 150 kHz) was mounted on the other end of the guide beam.

Thermo-acoustic emission during heating and cooling cycles was measured by an apparatus consisting of an electric furnace, a wave guide and the AE measuring system (Mistras-2001, Physical Acoustic Corp.), as shown in Fig. 3. A specimen in the furnace was heated from room temperature to 170℃ at the rate of +4.3℃/min and then was naturally cooled in the open furnace to room temperature. The cooling time was 1.5 hour. The thermal heating and cooling cycles were repeated three times. The AE measurement conditions were as follows: Pre-amplification 40 dB and threshold level 35 dB. The acoustic emis sion ring-down count rate, hit event counts, amplitude distribution, and time-amplitude signals were obtained from this measurement.

2.3 Ultrasonic C-scan

An water-immersion type ultrasonic C-scan apparatus was utilized for observation of a two-dimensional image of the internal damage distributions in the specimen. The back echo amplitude was scanned over the specimen by placing the ultrasonic focal point at a constant depth near the upper surface. The ultrasonic transducer was

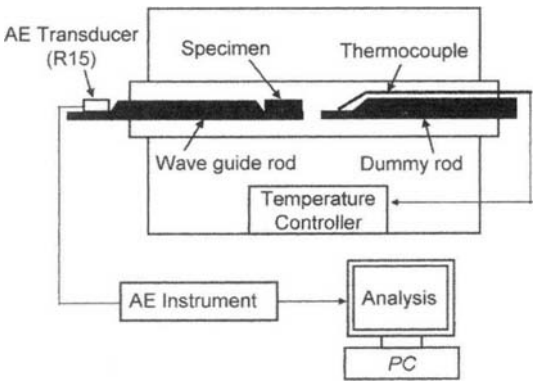

Fig. 3 Schematic of thermo-AE experimental apparatus

a focusing type, emitting a longitudinal wave of 15 MHz. Its scanning distance and focal point area were 0.085 mm and 0.1 mm, respectively.

2.4 Microscopic fractography

Using a low-speed diamond wheel cutter (ISOMET, Buehler Co.), specimens for optical microscopic observation were extracted from the specimen part which had been confirmed as a cryogenically-damaged region by the ultrasonic C-scan. Some artifacts caused by cutting were eliminated by polishing. The microstructure and failures of the specimens were observed using a reflection optical microscope. In addition, the delamination area of the specimen by cryogenic cooling was sectioned with a low-speed cutter to investigate the mechanism of microfractures appeared on the delamination area. The part was washed and then examined using a scanning electron microscope (SEM).

3. Analysis of Thermo-Acoustic Emission Behavior

3.1 Thermo-acoustic emission during the 1st thermal cycle

Figure 4(a) and (b) show the characteristics of the AE ring-down count rates obtained from untreated and cryogenically-treated $[+45_6/-45_6]_s$ specimens under the 1st thermal cycle, respectively. For the untreated specimen, the number of measured AE ring-down count was very small. However, numerous AE ring-down counts were detected from the cryogenically-treated specimen during the thermal cycle. This may indicate that many sources of AE generation, presumably,

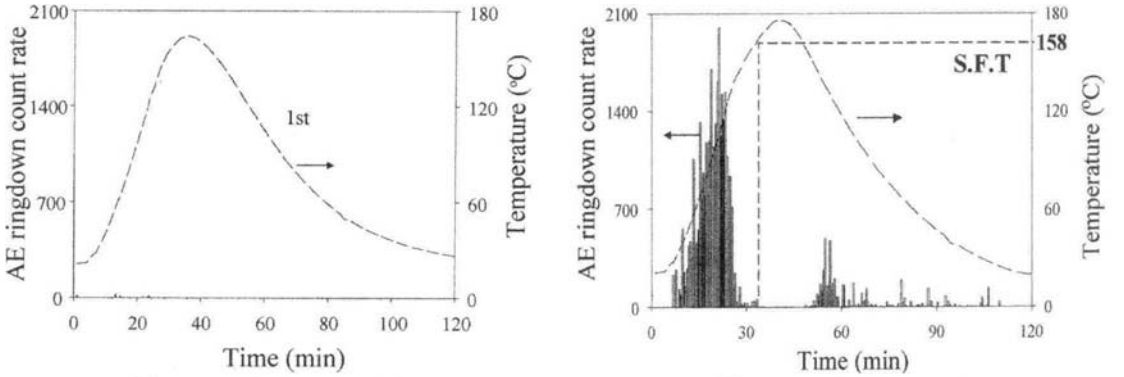

Fig. 4 Behavior of the AE ringdown count rate from $[+45_6/-45_6]_s$ specimens

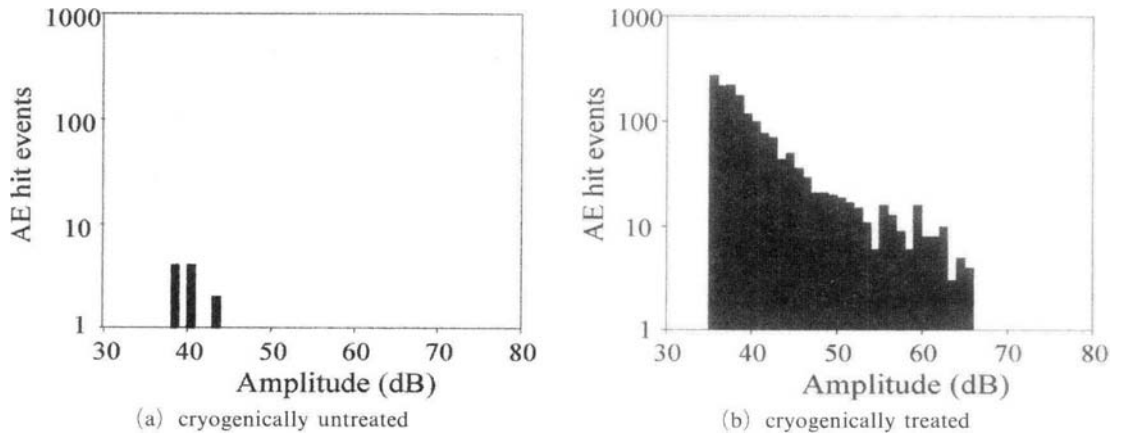

Fig. 5 Behavior of the AE hit events versus amplitude distribution from $[+45_6/-45_6]_s$ specimens

cracks and/or microfailures existed in the specimen. While emissions from the untreated specimen had low amplitudes below 43 dB (Fig. 5 (a)), the cryogenically-treated specimen generated rather high-energy emissions with the amplitudes up to 65 dB (see Fig. 5(b)). This may suggest that many large cracks were formed during the cryogenic cooling. During the 1st thermal cycle, it is thought that some frictional contact and/or abrasion arose between zig-zagged crack surfaces, moving by thermal deformation mismatch between plies, possibly generating rather strong emissions. Since each crack and microfailure in a specimen is apt to generate different emissions the analysis of thermo-AE behavior during the 1st thermal cycle may offer some significant indications on nondestructive evaluation of the composites.

3.2 Evaluation of the stress free temperature

Based on the thermo-AE behavior of the damaged laminate specimens in Fig. 4(b), the stress-free temperature (S.F.T.) (Griffin, 1983) may be evaluated during the 1st thermal cycle. Assuming that at the stress-free temperature is a stress-free state without mismatch of thermal deformation between the plies at that temperature, there may be several tentative ways to determine the stress-free temperature of fiber composites. It could be the curing temperature (170℃), if it is just below and/or similar to the glass transition temperature of the matrix resin, the pre-curing temperature (135℃) or an apparent deformation-free temperature measured from the laminate with the asymmetrical lay-up of $[+45_6/-45_6]$ using an oil-bath with a temperature controller. This asymmetrical laminate plate revealed significant warpage at room temperature, but exhibited a flatness (no warpage) at the temperature of about 120℃. Another way to determine the stress-free temperature is to adopt an AE-free temperature which can be measured during the heating period.

An illustrative example for determining the thermo-AE free temperature is also shown in Fig. 4(b). During the heating period, very high ringdown count rates were seen with an increase of the temperature up to 139℃. Beyond 139℃, however, the ringdown count rate was drastically decreased. As the temperature increased beyond 158℃, no emissions were generated. This may indicate that frictional contact between crack surfaces hardly arose, which might be on account of little mismatch of thermal deformation between plies with different fiber orientations (i.e. with different thermal expansion coefficients). Therefore it is thought that the stress-free temperature of the composite laminate may be equal to or above the lowest AE-free temperature (158℃).

Table 1 Estimated stress-free temperatures

Method	Estimated temperature (℃)
Acoustic emission-free	$\geq 157^{+4}_{-4}$
Apparent deformation-free	120
Pre-curing temperature	135
Curing temperature	170

Table 1 shows the measured values of the lowest AE-free temperature in comparison with the apparent deformation-free, pre-curing and curing temperatures. Although the absolute deviation in the measured values of lowest AE-free temperature was ±4℃ from the average (158℃) at the present experimental condition, the lowest AE-free temperatures were between the pre-curing and curing temperatures. Since at the pre-curing temperature, an amount of hardening occured in the epoxy resin during the removal of voids in the prepreg based on a vacuum suction state (Geier, 1994), the true stress-free temperature may be considered below the curing temperature. It is thus concluded that the exact stress-free temperature is between the lowest AE-free and the curing temperatures.

3.3 Kaiser effect during repetitive thermal cycles

In Fig. 4(b), the AE ring-down count rates during the cooling period were drastically reduced, compared to those of the heating. Furthermore, as shown in Fig. 6, the 2nd and 3rd thermal cycles resulted in additional decreases in the ring-down count rate. The maximum value of

the ring-down count rate in each thermal cycle had a tendency to decrease as an exponential function of the negative order number of thermal load cycles. Amplitudes of AE also fell below one-tenth during the repetitive thermal cycles (Fig. 7). Considering that the respective thermal cycles have the same thermal loading conditions in the temperature range as well as in the heating and cooling rates, the reduction in the ring-down count rate due to the repetitive heating and cooling indicates the thermal Kaiser effect. This behavior of thermo-AE may represent that through the repetitive thermal cycles, first, cracks in the specimen did not propagate further and, second, weakening of frictional contact forces between crack surfaces due to relaxation of accumulated residual stresses brought about a decrease in secondary abrasive microfractures.

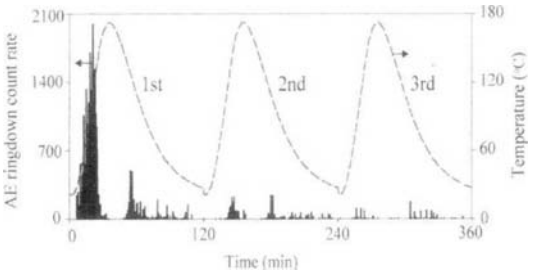

Fig. 6 Behavior of the AE ringdown count rate from a cryogenically treated specimen of $[+45_6/-45_6]_s$ during the repetitive thermal load cycles

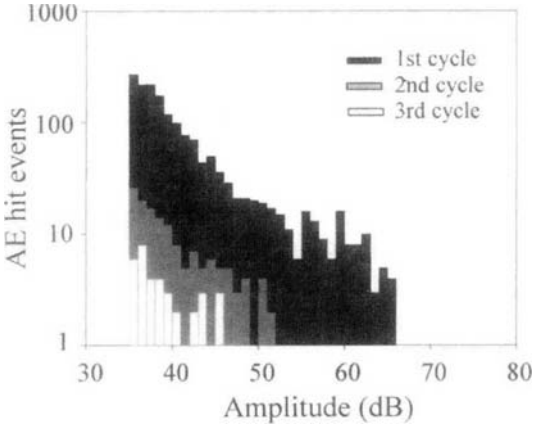

Fig. 7 AE hit events versus amplitude distributions during the repetitive thermal load cycles

4. Microscopic Fracture Morphology

Figure 8 shows an ultrasonic C-scan image obtained from the cryogenically-treated $[+45_6/-45_6]_s$ laminate specimen. The dark image indicating some delaminated region appears in the corner region A, where the maximum interlaminar stress took place during the cryogenic treatment as reported (Lee et. al., 1999 ; Choi and Lee, 2001). Many local dark regions were distributed within a range of about 21 mm from the corner site of the laminate. Such an image of damage was hardly observed by the C-scan for the as-molded specimens. Figure 9 is an optical

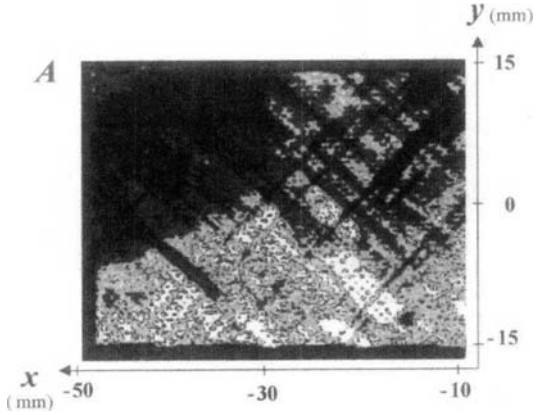

Fig. 8 Ultrasonic C-scan image of a cryogenically treated $[+45_6/-45_6]_s$ laminate. Dark image indicates cryogenic damages

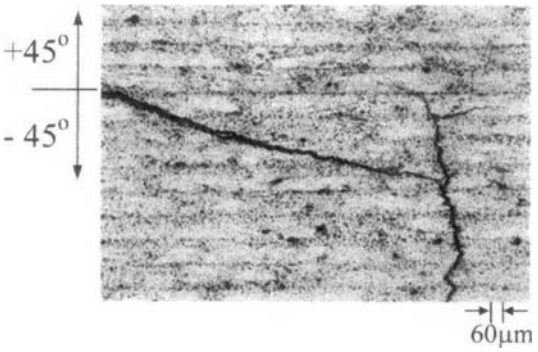

Fig. 9 Microscopic photograph of the cross-section near the free edge of a $[+45_6/-45_6]_s$ laminate. Several transverse cracks and delaminations are revealed

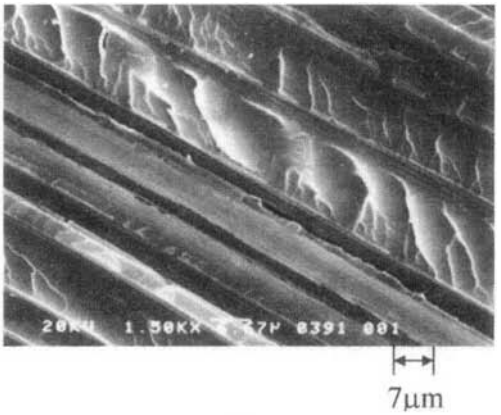

(a)

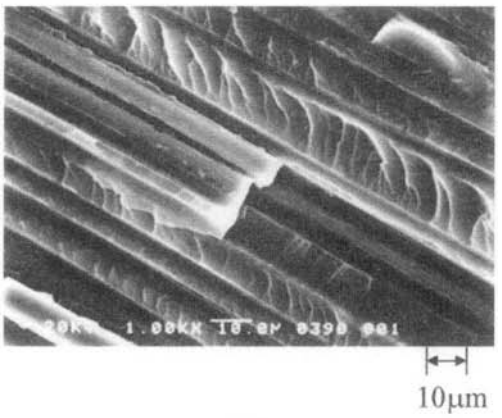

(b)

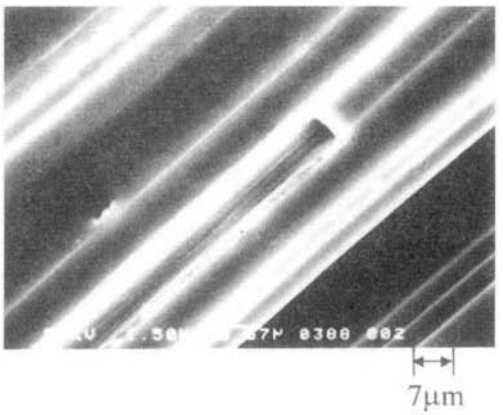

(c)

Fig. 10 SEM photographs of various failure types in cryogenically treated $[+45_6/-45_6]_s$ laminates: (a) type I, a fracture of the matrix and/or interfaces. (b) type II, a simultaneous fracture of fibers and matrix. (c) type III, a fiber breakage

micrograph of the cross-section of the damaged free edge region (near x=−50 mm, y=−5 mm) in Fig. 8, exhibiting an interlaminar region between the skin layer with +45° fibers and the core layer with −45° fibers. Due to the cryogenic cooling, the delamination crack near the +45°/−45° ply interface took place inducing a biased local crack propagating into the core layer, which joined with the transverse crack arisen from the core layer. Those cracks propagated in a zig-zagged way through the matrix resin and around the fiber-matrix interfaces, which might cause fracture of fibers bridged across the crack path.

Figure 10 shows SEM photograph taken from the fracture surface corresponding to the delaminated portion of a $[+45_6/-45_6]_s$ specimen subjected to cryogenic cooling. A type-I fracture observed in Fig. 10(a) is a typical fracture of the matrix and/or interfaces. This may have generated AE waves with low frequencies and low amplitudes (Weng et. al., 1990; Choi et. al., 1992; Choi and Takahashi, 1998). Figure 10(b) exhibits a type-II fracture which is a simultaneous fracture of fibers and matrix. It is supposed that most type II fractures were formed due to the large buildup of high interlaminar and in-plane tensile stresses in the corner region during the sudden temperature drop of the initial stage of cryogenic cooling. This type of fracture which is accompanied by fiber breakages is liable to generate strong emissions with high energy in a mixture of high and low frequencies (Choi et. al., 1992; Choi and Takahashi, 1998). Figure 10(c) shows fracture type III, i.e. a fiber breakage with little debris of a matrix fracture. This might generate strong AE with dominantly high frequencies.

5. Thermo-AE Monitoring and Evaluation

AE sources during the fracture of fiber composites are considered to be matrix fractures, fiber-matrix interfacial cracking, fiber breakage and fiber pull-out (Weng et. al., 1990; Choi et. al., 1992; Choi and Takahashi, 1998), which may generate emissions with different frequency bands

and different amplitudes according to the individual fracture types and modes. To investigate the fracture processes occurring in the specimen, each AE signal detected from the specimen was processed in a personal computer system using a time-frequency analysis method of the short-time Fourier transform programmed by the commercial software MATLAB 5.3. As exhibited in Figure 11(a) to (c), AE signals measured during the 1st thermal cycle were classified into three types. The type-I signals had a low frequency band of 70-200 kHz (Fig. 11(a)), the type-II signals had both low and high frequency bands of 70-500 kHz (Fig. 11(b)), and the type-III signals had a dominantly high frequency band of 200-500 kHz (Fig. 11(c)). Histograms along the right side of Fig. 11(a) to (c) indicate the intensity of the signals. Considering that a matrix and/or interfacial fracture generates emission of the low frequency band (Choi et. al., 1992; Choi and Takahashi, 1998), it is thought that the type-I signals were generated from secondary microfractures in the matrix contacting between moving crack surfaces. Because a fiber fracture is liable to produce emissions of the high frequency band (Choi et. al., 1992; Choi and Takahashi, 1998), it is supposed that the type-III signals were emitted from some abrasive fracturing of broken fiber ends between upper and lower crack surfaces shown in Fig. 10(b). The type-II signals seem to have been generated from fiber fracturing accompanied by the matrix microfracture.

Fig. 12 shows that the type-I signals were very dominant in the total AE hit events detected during the 1st thermal cycle. As the same thermal cycle was repeatedly applied to the cryogenically-treated specimen, the number of the type-I hit events decreased almost exponentially. The repetitive cycles caused the type-II events to occur far less frequently. Most secondary abrasive microfractures seem to have not been any further propagated. It may be understood that the type-I events correspond to some secondary abrasive

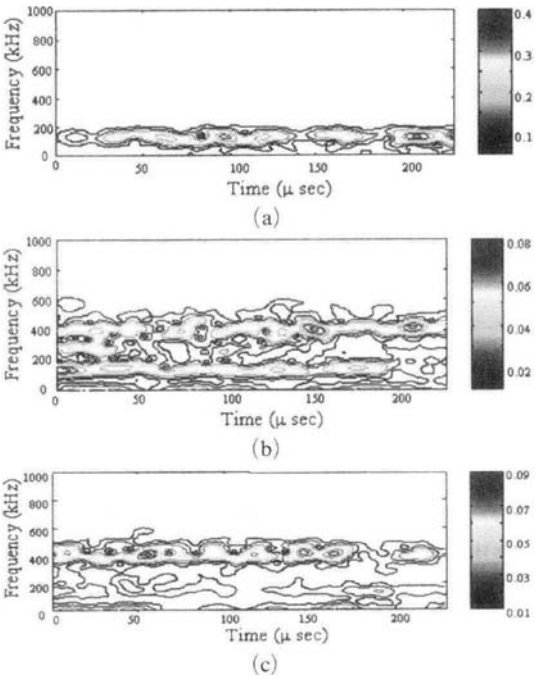

Fig. 11 Classification of thermo-AE signals: (a) Type I AE (low frequency band), (b) type II AE (low and high frequency band) and (c) type III (high frequency band). Three different types of thermo-AE signals were obvious, which may be related with abrasive micro-fracture processes in the matrix and fiber end parts during thermal load cycle

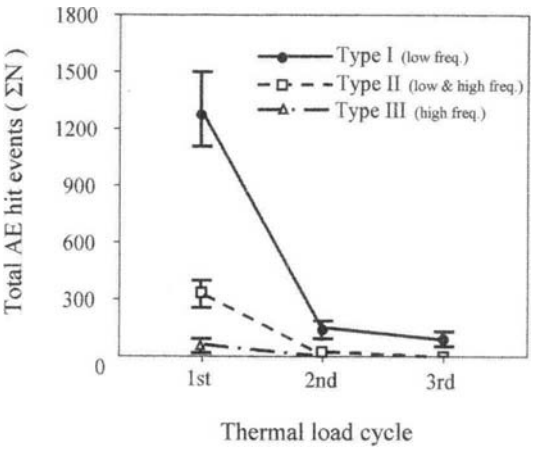

Fig. 12 Total AE ring-down counts ($\sum$N) obtained from cryogenically-treated $[+45_6/-45_6]_s$ laminates according to the three types of AE signals for each repetitive thermal load cycle. Type I signals were very dominant, but largely decreased in number during the repetitive thermal cycles

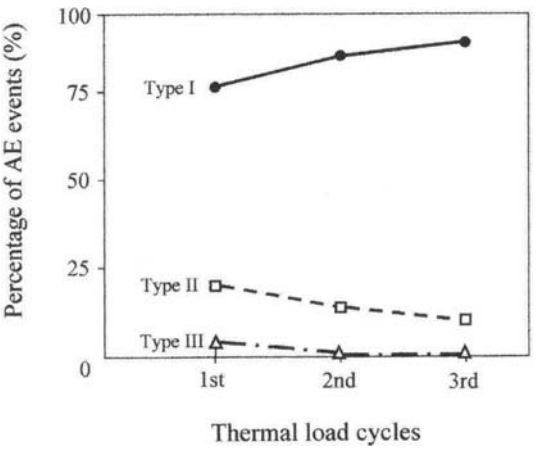

Fig. 13 Relative percentage of the total AE hit events according to the three types of AE signals detected during each thermal load cycle. These data were calculated from those in Fig. 12. Percentage of the signal type may be a nondestructive indicator for the amount of each type of fractures in cryogenically-treated composites

microfractures in matrix, since such high percentage (about 76%) of the type-I signals shown in Fig. 13 is related with a large fraction of cryogenically-fractured portion of matrix over the total fracture surface as shown in Figs. 9 and 10. The repetitive cycles caused the percentage of the type-I signals to increase from 76% to about 87%. The type-II events were minor in quantity, but they occurred to a degree in the 1st thermal cycle. This may be a nondestructive indicator for how many fiber breakages had been formed during the cryogenic cooling.

6. Conclusions

The thermo-acoustic emission (AE) method has been applied to the nondestructive evaluation of fiber composite laminates subjected to a cryogenic cooling. Many emissions were observed for the cryogenically-treated composites, while few emissions were detected for the untreated ones. The Kaiser effect in the thermo-AE behavior was confirmed : A large reduction in the AE ring-down count rate and amplitudes was shown during the repetitive thermal cycles. On the basis of the thermo-AE behavior, the stress-free temperature of the composites was determined to lie between the curing and the lowest AE-free temperatures. The thermo-AE signals were processed with the short-time Fourier transform to be classified into three different types which correlated with such individual fracture processes as secondary microfracture of the matrix contacting between moving crack surfaces and/or abrasive contact between broken fiber ends. Analysis of the thermo-AE behavior through the heating and cooling cycles enabled to present nondestructive estimation of the cryogenic damages of composites.

Acknowledgment

This work was supported by the Brain Korea 21 Project as well as Korea Research Foundation Grant(KRF-2000-E00058).

References

Choi, N. S. and Takahashi, K., 1998, "Characterization of the Damage Process in Short-Fibre/Thermoplastic Composites by Acoustic Emission," *Journal of Materials Science*, Vol. 33, pp. 2357~2363.

Choi, N. S. and Lee, S. H., 2001, "Nondestructive Evaluation of Thermal Stress-Induced Damage in Thin Composite Laminates," *Journal of Materials Science*, Vol. 36, No. 7, pp. 1685~1693.

Choi, N. S., Takahashi, K. and Hoshino, K., 1992, "Characteristics of Acoustic Emission during the Damage Process in Notched Short-Fiber-Reinforced Thermoplastics," *NDT & E International*, Vol. 25, pp. 271~278.

Geier, M. H., 1994, "Quality Handbook for Composite Materials," Chapman & Hall, London, pp. 142~152.

Griffin, O. H., Jr., 1983, "Three-Dimensional Curing Stresses in Symmetric Cross-Ply Laminates with Temperature-Dependent Properties," *Journal of Composite Materials*, Vol. 17, pp. 449~463.

Lee, S. H., Choi, N. S. and Lee, J. K., 1999,

"Vibration-based Nondestructive Evaluation of Thermal Stress-Induced Damage in Thin Composite Laminates," *Journal of the Korean Society for Nondestructive Testing*, Vol. 19, pp. 347~355.

Sato, N., Kurauchi, T. and Kamigaito, O., 1988, "Detection of Damage in Composite Materials by Thermo-Acoustic Emission Measurement," *Journal of Composite Materials*, Vol. 22, pp. 447~458.

Standard Practice for Acoustic Emission Examination of Fiberglass Reinforced Plastic Resin (FRP) Tanks/Vessels, ASTM Designation: E1067-01, American Society for Testing and Materials, West Conshohocken, PA, (July, 2001).

Standard Practice for Acoustic Emission Examination of Reinforced Thermosetting Resin Pipe (RTRP), ASTM Designation: E1118-00, American Society for Testing and Materials, West Conshohocken, PA, (December, 2000).

Weng, T., Hiltner, A. and Baer, E., 1990, "Damage Analysis in Reinforced LCP Composites by Acoustic Emission Location Techniques," *Journal of Composite Materials*, Vol. 24, pp. 103-121.